Perturbative representation of ultrashort nonparaxial elegant Laguerre-Gaussian fields

Andrew Vikartofsky, Anthony F. Starace, and Liang-Wen Pi

Phys. Rev. A **98**, 043820 — Published 10 October 2018

DOI: 10.1103/PhysRevA.98.043820

Perturbative Representation of Ultrashort Nonparaxial Elegant Laguerre-Gaussian Fields

Andrew Vikartofsky and Anthony F. Starace
Department of Physics and Astronomy, The University of Nebraska, Lincoln, Nebraska 68588-0299, USA

Liang-Wen Pi*
Max Planck Institute for the Physics of Complex Systems, Nöthnitzer Straße 38, 01187 Dresden, Germany
(Dated: September 17, 2018)

An analytical method for calculating the electromagnetic fields of a nonparaxial elegant Laguerre-Gaussian (LG) vortex beam is presented for arbitrary pulse duration, spot size, and LG mode. This perturbative approach provides a numerically tractable model for the calculation of arbitrarily high radial and azimuthal LG modes in the nonparaxial regime, without requiring integral representations of the fields. A key feature of this perturbative model is its use of a Poisson-like frequency spectrum, which allows for the proper description of pulses of arbitrarily short duration. This model is thus appropriate for simulating laser-matter interactions, including those involving short laser pulses.

I. INTRODUCTION

The ability to produce vortex beams of light [1–4] or electrons [5–7] with well-defined orbital angular momentum allows for the study of angular momentum exchange processes when such beams interact with matter. Recently, optical vortex (or "structured light") beams have been used to probe chiral matter [8], to study multipole excitation of atoms as a function of their location with respect to the beam axis [9], to improve vacuum acceleration of electrons [10], and to advance quantum information technologies [1, 11], among numerous other applications. Such structured light can be created in the extreme ultraviolet by means of high-order harmonic generation [12–14]. For some applications of optical vortex beams, high intensity is required (such as, e.g., for vacuum acceleration of charged particles [10]), which is usually achieved by tightly focusing the beam. However, tightly-focused beams with spot sizes comparable to the laser wavelength cannot be correctly described within the paraxial approximation [15, 16].

Perturbative solutions for the fields beyond the lowest-order paraxial approximation were considered as early as 1975, in which the first few orders of nonparaxial corrections were found [16–18]. The first order correction introduces a longitudinal electric field, which is absent in the paraxial approximation. Many higher order corrections to the electromagnetic (EM) fields have since been found [19, 20].

Perturbative solutions of the scalar Helmholtz equation (HE) (whose exact solution is termed the phasor) provide an alternative approach for treating nonparaxial effects. Solutions for the HE phasor have been obtained primarily by two different methods. One method involves solving for the exact phasor in integral or differential form. This phasor is then expanded perturbatively [18, 21, 22]. Alternatively, the HE can be solved one perturbative order at a time, and an exact phasor built from the sum of these solutions [17, 23–25]. With either of these two methods, the HE can be solved under different sets of boundary conditions [26]. Common choices for boundary conditions include: (i) a purely paraxial beam in the focal plane [18, 24, 25] (where the exact solution is valid in the half space after the focus only, while the perturbative solution is valid in all space), (ii) an oscillatory far-field beam [17, 19], or (iii) an outgoing spherical wave in the far-field [21–23]. Couture and Belanger [23] showed that the latter, with infinitely many orders of correction, was equivalent to modeling the Gaussian beam with a so-called complex *source-point*.

The complex source-point model warrants additional discussion. It describes the beam as an outgoing spherical wave originating from an imaginary point on the optical axis. The phasor described by this model has a circular singularity in the focal plane since the imaginary location of the point source is related to a circle in real space [27, 28]. A boundary condition of far-field counter-propagating spherical waves was implemented to remove the singularity in the complex source-point model [28–31]. This is known as the complex *source-sink* model, with the source and sink at the same imaginary location along the optical axis. While the singularity is removed in this model, the energy density diverges logarithmically as the transverse coordinate grows large [32]. It has been stated, however, that this energy divergence is irrelevant in practice since neither experiments nor simulations look to sufficiently large transverse distance for it to matter [33, 34].

As our aim in this paper is to describe tightly-focused optical vortex beams carrying orbital angular momentum, we utilize henceforth Laguerre-Gaussian (LG) models of such optical beams. In general, LG beams are classified by two indices $LG_{n,m}$, with n and m representing the radial and azimuthal profiles, respectively. These are referred to as the LG "modes," of which the lowest order is a Gaussian beam and higher orders can describe

* lwpi@pks.mpg.de

vortex beams. In particular, we utilize the so-called elegant LG (eLG) model, wherein the arguments of certain special functions are complex variables. Note that there is a physical difference between LG and eLG models, as discussed by Saghafi and Sheppard [35]. Bandres and Gutiérrez-Vega (BGV) have provided exact integral and differential solutions for monochromatic eLG beams of any LG mode (see Eqs. (16) & (21) of Ref. [22]). These solutions, based on the complex *source-point* model, contain the singularity discussed above. In Ref. [22], BGV presented an equally general perturbative solution which does not contain the singularity, since a truncated perturbative model does not exactly satisfy the source-point boundary condition (see Eq. (24) of Ref. [22]). As an alternative approach, April employed a closed-form *source-sink* model for monochromatic eLG fields in Ref. [31] that is singularity-free.

Nearly all of the analytical models discussed thus far entail a significant limitation: they assume a monochromatic beam. Many modern experiments, particularly those studying high intensity laser-matter interactions, involve optical pulses, shaped pulses, chirped pulses, etc., all of which require a polychromatic description. While long pulses can be well approximated as the product of a temporal Gaussian envelope and a monochromatic field, this description becomes inadequate for ultrashort pulses [36]. Others have employed polychromatic descriptions, but these often assume that k_z is frequency-independent or involve non-LG models (see, e.g., Refs. [37–39]). April [40] generalized his source-sink model [31] for monochromatic eLG fields to allow for polychromatic descriptions by introducing a Poisson-like frequency spectrum [41, 42]. Application of the Hertz potentials [43, 44] then allowed the computation of a complete set of EM fields for an arbitrarily short pulse duration and any LG mode. These fields are free of all singularities [30], and can be made free of all discontinuities [45], which are present in the complex source-point models. While Ref. [40] presents a complete model for describing eLG pulses in the frequency domain, the Fourier transform required to achieve a time-domain phasor, and therefore the EM fields, is nontrivial. To our knowledge, this integral has only been carried out for the lowest radial order $n = 0$ in Ref. [45]. Due to a sum over radial orders in the frequency-domain phasor of Ref. [40], the Fourier transform for higher radial modes becomes increasingly complicated to calculate.

In this paper we present an analytical method for calculating the time-domain phasor, and EM fields, of a tightly-focused, arbitrarily-short pulse for any LG mode. Our method generalizes the perturbative approach of BGV [22] by including a Poisson-like frequency spectrum and calculating the EM fields from the time-domain phasor. We show that our fields agree with those generated from the model of Refs. [40, 45] for the $n = 0$ case, and that fields for higher order LG modes can easily be produced. The primary advantage of this method over that proposed in Ref. [40] is the ability to obtain an explicit expression for the time-domain phasor, thus enabling one to obtain the EM fields by a straightforward prescription.

This paper is organized as follows. In Section II we derive the time-domain phasor used to calculate the EM fields. In Section III we derive general expressions for these EM fields, which are valid for any LG mode and for any order of perturbative correction to the phasor. In Section IV we present a test of the convergence of our perturbative results and examine the necessity of the temporal model we employ. In Section V we summarize our results and present our conclusions and outlook. In Appendices A and B we present some details of our derivations, and in Appendix C we determine the spatial radius of convergence for this perturbative model.

II. THE PHASOR

The derivation of our phasor (the spatiotemporal solution to the scalar HE [46]) begins with the frequency-domain perturbative phasor of BGV (Eq.(24) of Ref. [22]) in cylindrical polar coordinates,

$$
\begin{aligned}
U_{BGV}(\mathbf{r},\omega) &= (-1)^{n+m} 2^{2n+m} \exp(ikz + im\phi) \\
&\quad \times h^{2n+m+2} v^{m/2} \exp(-v) \\
&\quad \times \sum_{j=0}^{N} \left(\frac{h^2}{k^2 \mathrm{w}_0^2}\right)^j f_{n,m}^{(2j)}(v) \\
&\equiv U_{0,BGV} + \frac{\epsilon^2}{\beta}\, U_{2,BGV} + \frac{\epsilon^4}{\beta^2}\, U_{4,BGV} + \ldots
\end{aligned}
\tag{1}
$$

where $\epsilon \equiv 1/(k\mathrm{w}_0)$ is a small dimensionless parameter, $h = (1 + iz/z_R)^{-1/2}$, $\beta = 1/h^2$, $v = h^2\rho^2/\mathrm{w}_0^2$, w_0 is the beam waist, $z_R = k\mathrm{w}_0^2/2$ is the Rayleigh length, and N is the term at which the infinite series is truncated. The factors $f_{n,m}^{(2j)}(v)$ can be obtained from Eqs. (25) of Ref. [22] (as discussed in detail in Appendix A below). These factor are each linear combinations of associated Laguerre polynomials $L_n^m(v)$, and can be found to any order using the results in Ref. [22].

If we were to evaluate the perturbative expansion of the phasor in Eq. (1) to infinite order (i.e., $N \to \infty$), this would be equivalent to describing wave emission from a complex point source (cf. Ref. [23]). The singularity that naturally arises from this point source, however, is avoided by our truncation of the perturbative expansion at some finite order N. This truncation is equivalent to approximating the source-point spherical wave, an effect of which is that we have a singularity-free model. As such, the incoming spherical waves employed in other works are not required to cancel a source-point singularity in our model.

Keeping terms up to order ϵ^2, the sum in the phasor of Eq. (1) reduces to

$$\sum_{j=0}^{1}\left(\frac{h}{k\mathrm{w}_0}\right)^{2j} f_{n,m}^{(2j)}(v) = n! L_n^m(v) + \frac{\epsilon^2}{\beta}\Big[\, 2(n+1)! L_{n+1}^m(v) - (n+2)! L_{n+2}^m(v)\,\Big]. \tag{2}$$

In Eq. (2), the associated Laguerre polynomials $L_n^m(v)$ can be expressed as finite sums [47],

$$L_n^m(v) \equiv \sum_{j=0}^{n} G_{n,m,j}\; v^j, \tag{3}$$

in which

$$G_{n,m,j} \equiv \frac{(-1)^j (n+m)!}{(n-j)!(m+j)!j!}. \tag{4}$$

Since the BGV phasor was derived for the case of a monochromatic field, in order to describe a temporally finite pulse it must be generalized. We accomplish this by multiplying the BGV phasor by a Poisson-like frequency spectrum [41, 42],

$$f(\omega) = 2\pi e^{i\phi_0}\left(\frac{s}{\omega_0}\right)^{s+1}\frac{\omega^s \exp(-s\omega/\omega_0)}{\Gamma(s+1)}\Theta(\omega), \tag{5}$$

where s is the spectral parameter controlling the pulse duration, ω_0 is the central frequency, ϕ_0 is the initial phase of the pulse, $\Gamma(s+1)$ is a gamma function, and $\Theta(\omega)$ is the unit step function. Our polychromatic frequency-domain phasor is then defined as,

$$U(\mathbf{r},\omega) \equiv U_{BGV} f(\omega). \tag{6}$$

In the limit of a narrow spectrum, $s \gg 1$, Eq. (5) reduces to a Gaussian spectrum with pulse duration $\tau = \sqrt{2s}/\omega_0$.

In order to Fourier transform the phasor in Eq. (6) to the time domain, we adopt the condition of isodiffraction, i.e., we assume that every frequency component has the same wavefront radius of curvature. For this choice of complex source-point location, the isodiffraction condition ensures that z_R is constant for all frequency components, whereas the beam waist, $\mathrm{w}_0 = \sqrt{2z_R/k}$, depends on ω through the vacuum dispersion relation $k = \omega/c$, where c is the speed of light [41, 42, 48].

Owing to the introduction of a Poisson-like frequency spectrum to the monochromatic phasor of BGV, implementation of the smallness parameter must be modified slightly. Since ϵ now varies with the frequency, we can use its definition to factor out its frequency dependence,

$$\epsilon^2 = \frac{c}{2z_R\omega} = \frac{c}{2z_R\omega_0}\frac{\omega_0}{\omega} \equiv \epsilon_c^2\frac{\omega_0}{\omega}, \tag{7}$$

where ϵ_c is a frequency-independent (constant) small parameter in terms of the central pulse frequency, ω_0.

With all frequency dependencies accounted for, one can now Fourier transform $U(\mathbf{r},\omega)$ into the time domain,

$$U(\mathbf{r},t) = \frac{1}{\sqrt{2\pi}}\int_{-\infty}^{\infty} U(\mathbf{r},\omega)\exp(-i\omega t)\mathrm{d}\omega, \tag{8}$$

where the negative exponential is chosen so that the resulting pulse is traveling in the $+\hat{\mathbf{z}}$-direction. Using the integral representation of the gamma function (cf. Eq. (6.1.1) of [49]),

$$\Gamma(\gamma+1) = \eta^{\gamma+1}\int_0^{\infty}\mathrm{d}\omega\,\omega^{\gamma}\exp(-\eta\omega), \quad Re\,\eta > 0, \tag{9}$$

we obtain the time-domain phasor (by methods shown explicitly in Appendix B),

$$U(\mathbf{r},t) = \Lambda_{n,m}\left[\sum_{j=0}^{n} c_{0,0}\xi^j T^{-(\gamma+1)} + \frac{\epsilon_c^2}{\beta}\left(\sum_{j=0}^{n+1} c_{1,1}\xi^j T^{-\gamma} - \sum_{j=0}^{n+2} c_{1,2}\xi^j T^{-\gamma}\right)\right]. \tag{10}$$

The new variables in Eq. (10) are defined as

$$\xi \equiv \frac{\rho^2}{2c\beta z_R} \tag{11a}$$

$$T \equiv 1 + \frac{\omega_0}{s}\left(-\frac{iz}{c} + \xi + it\right) \tag{11b}$$

$$\Lambda_{n,m} \equiv (-1)^{n+m}2^{2n+m}\sqrt{2\pi}n!\exp(i\phi_0) \times \xi^{m/2}\beta^{-(n+m/2+1)}\exp(im\phi), \tag{11c}$$

and the constants are defined as

$$c_{0,0} \equiv G_{n,m,j}\left(\frac{\omega_0}{s}\right)^{\gamma-s}\frac{\Gamma(\gamma+1)}{\Gamma(s+1)} \tag{12a}$$

$$c_{1,1} \equiv (n+1)G_{(n+1),m,j}\left(\frac{\omega_0}{s}\right)^{\gamma-s-1}\frac{2\omega_0\Gamma(\gamma)}{\Gamma(s+1)} \tag{12b}$$

$$c_{1,2} \equiv \omega_0(n+1)(n+2)G_{(n+2),m,j}\left(\frac{\omega_0}{s}\right)^{\gamma-s-1} \tag{12c}$$

$$\times\frac{\Gamma(\gamma)}{\Gamma(s+1)} \tag{12d}$$

$$\gamma \equiv m/2 + s + j. \tag{12e}$$

Further details of this derivation can be found in Appendix B.

III. THE FIELDS

From the expression for the phasor $U(\mathbf{r},t)$ in Eq. (10), Hertz potentials [43, 44] can be used to generate expressions for the complex EM fields. The desired polarization of the laser field is determined by the form of these Hertz potentials, and not from any property of the phasor. As an example, for the case of radial polarization the EM fields can be expressed from the phasor as simply

$$\mathbf{E}(\mathbf{r},t) = \nabla \times \nabla \times (U(\mathbf{r},t)\hat{\mathbf{z}}) \tag{13a}$$

$$\mathbf{H}(\mathbf{r},t) = \epsilon_0 \frac{\partial}{\partial t} \nabla \times (U(\mathbf{r},t)\hat{\mathbf{z}}) \tag{13b}$$

For different polarizations, these expressions for $\mathbf{E}$ and $\mathbf{H}$ would change (see Table 3 on p. 372 of Ref. [40] and the text at the bottom of p. 361 of Ref. [40] for more details).

In the expressions that follow for the unnormalized EM fields, we have carried out calculations for all but the most simple partial derivatives of the phasor. By leaving these derivative terms in the field equations, we ensure that the expressions remain valid for higher perturbative orders in which the phasor is modified to have additional terms.

$$\begin{aligned} E_\rho = -\frac{i}{\rho}\Bigg\{ & \frac{m(n+m+1)}{\beta z_R}U - \frac{2\omega_0 \xi}{s z_R}\frac{\partial^2 U}{\partial\beta\partial T} \\ & + \frac{\omega_0}{s}\left[\frac{2\xi(n+m+2)}{\beta z_R} + m\left(\frac{\xi}{\beta z_R}+\frac{1}{c}\right)\right]\frac{\partial U}{\partial T} \\ & + \frac{\xi(2n+3m+4)}{\beta z_R}\frac{\partial U}{\partial \xi} - \frac{m}{z_R}\frac{\partial U}{\partial \beta} \\ & + \frac{2\xi^2}{\beta z_R}\frac{\partial^2 U}{\partial \xi^2} + \frac{2\omega_0\xi}{s}\left(\frac{2\xi}{\beta z_R}+\frac{1}{c}\right)\frac{\partial^2 U}{\partial\xi\partial T} \\ & - \frac{2\xi}{z_R}\frac{\partial^2 U}{\partial\xi\partial\beta} + \frac{2\omega_0^2\xi}{s^2}\left(\frac{\xi}{\beta z_R}+\frac{1}{c}\right)\frac{\partial^2 U}{\partial T^2}\Bigg\} \end{aligned} \tag{14}$$

$$\begin{aligned} E_\phi = \frac{m}{\rho}\ \Bigg[& \frac{n+m+1}{\beta z_R}U + \frac{\omega_0}{s}\left(\frac{\xi}{\beta z_R}+\frac{1}{c}\right)\frac{\partial U}{\partial T} \\ & + \frac{\xi}{\beta z_R}\frac{\partial U}{\partial \xi} - \frac{1}{z_R}\frac{\partial U}{\partial\beta}\Bigg] \end{aligned} \tag{15}$$

$$\begin{aligned} E_z = \frac{\xi}{\rho^2}\Bigg\{ & -\frac{4\omega_0}{s}(m+1)\frac{\partial U}{\partial T} - 4(m+1)\frac{\partial U}{\partial \xi} \\ & -\frac{4\omega_0^2\xi}{s^2}\frac{\partial^2 U}{\partial T^2} - 4\xi\frac{\partial^2 U}{\partial \xi^2} - \frac{8\omega_0\xi}{s}\frac{\partial^2 U}{\partial\xi\partial T}\Bigg\} \end{aligned} \tag{16}$$

$$B_\rho = -\frac{m\omega_0}{c^2 s\rho}\frac{\partial U}{\partial T} \tag{17}$$

$$B_\phi = -\frac{i\omega_0}{c^2 s \rho}\left\{m\frac{\partial U}{\partial T} + 2\xi\left(\frac{\omega_0}{s}\frac{\partial^2 U}{\partial T^2} + \frac{\partial^2 U}{\partial\xi\partial T}\right)\right\} \tag{18}$$

As is the case with all radially polarized fields, $B_z = 0$. The perturbative order necessary to achieve convergence will be discussed in the next section.

IV. RESULTS

A. Test for Accuracy of Fields Obtained from the Perturbative Phasor

Depending on the parameters used to describe the optical field, perturbative orders higher than ϵ_c^2 may need to be included in the phasor. These higher order corrections are needed not only as the spot size is reduced, but also as the radial or azimuthal LG indices are increased. Numerical simulations show that excluding terms above order ϵ_c^2 is sufficient only for the lowest LG modes.

A simple method for checking the convergence of the perturbative expansion of the phasor is to verify that the wave equation is satisfied to within some numerical tolerance. Since the phasor must be a solution to the wave equation [40], we can write explicitly

$$\nabla^2 U = \frac{1}{c^2}\frac{d^2}{dt^2}U. \tag{19}$$

One can check directly that the equation is satisfied at any given order of perturbation. If an appropriate perturbative order is used to represent the phasor, numerical comparison of $|\nabla^2 U|$ and $|\partial_t^2 U/c^2|$ will agree, since the wave equation will be satisfied. Disagreement, on the other hand, indicates that additional terms in the perturbative expansion must be included in order to achieve a converged phasor. We note that since all fields are calculated as derivatives of the phasor, use of Eq. (19) to check the adequacy of the perturbative expansion is valid for any field polarization, not just for the radially polarized fields calculated above as an example.

To illustrate this technique, a comparison of the left- and right-hand sides of Eq. (19) is shown in Fig. 1 for three LG modes, calculated for two different orders of perturbative correction. For each of the results in Fig. 1, we present the root mean squared error (RMSE) between $|\nabla^2 U|$ and $|\partial_t^2 U/c^2|$ calculated using 200 plot points across the range of ρ/λ shown. Convergence of the perturbative expansion can be claimed if the RMSE is sufficiently small (the exact definition of which depends on the application). The results in Figs. 1(d) - 1(f) show improved agreement between the left- and right-hand sides of the wave equation over those in Figs. 1(a) - 1(c), respectively, as the order of perturbation increases from $O(\epsilon_c^2)$ to $O(\epsilon_c^4)$. However, agreement between these terms becomes worse as the LG mode increases from $n = 2$ to $n = 3$ for both the phasors of $O(\epsilon_c^2)$ and those of $O(\epsilon_c^4)$, thus illustrating the need to check for convergence. Calculations for other LG modes having indices $n + m \leq 3$ (not shown) have RMSE values similar to those for the LG modes shown in Fig. 1 when corrections to similar perturbative orders are included.

We emphasize that the addition of higher order corrections to the phasor does not change the EM field equations that have been derived in Section III. The expressions for the EM fields given in Eqs. (14)-(18) remain

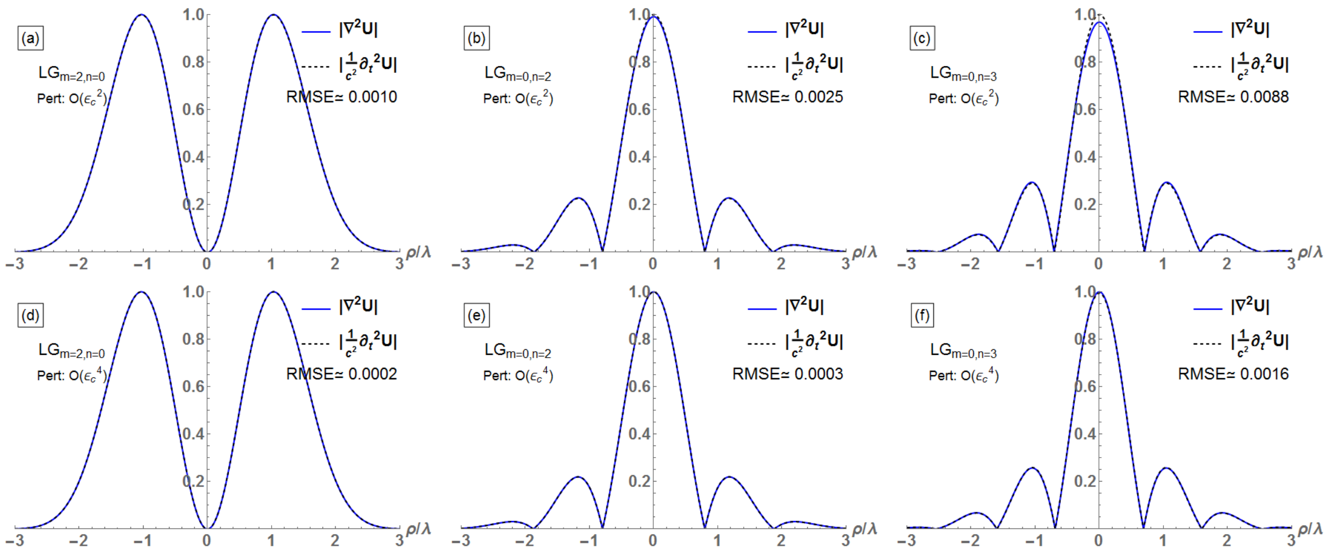

FIG. 1. Comparison of both sides of the wave equation [Eq. (19)] for the phasor, $|\nabla^2 U|$ and $|\partial_t^2 U/c^2|$, for three LG modes, calculated for two different orders of perturbative correction. Panels [(a),(d)] show LG mode $m = 2, n = 0$, panels [(b),(e)] show $m = 0, n = 2$, and panels [(c),(f)] show $m = 0, n = 3$. The phasor contains perturbation terms to order ϵ_c^2 in [(a)-(c)] and to order ϵ_c^4 in [(d)-(f)]. The RMS error decreases when the higher order term is included in the phasor. These plots were made near the beam waist using $s = 70$ and $\mathrm{w}_0 = \lambda = 800$ nm ($\epsilon_c^2 \approx 0.0253$).

valid as the phasor is modified, since these field expressions are written in terms of partial derivatives of the phasor. Thus, use of our field equations for higher perturbative orders is relatively straightforward, requiring only the addition of higher order corrections to the phasor. Appendix B provides an example in which the perturbative correction of order ϵ_c^4 is calculated in detail.

In Fig. 2 we compare our converged fields from Eqs. (14) and (16) with those obtained from the closed-form phasor of April [40]. The normalized electric field intensities in the $\hat{\rho}-$ and $\hat{\mathbf{z}}-$directions are shown for each model, for both long and short pulse durations. Excellent agreement is seen between the fields of our model (subscript "pert" in the figure) and those of April (subscript "A"), for both long (Fig. 2a) and short (Fig. 2b) pulses. The spatial radius of convergence of the perturbative expansion is discussed in Appendix C.

B. Sensitivity of the Fields to the Spectral Profile

The EM fields are calculated using the time-domain phasor $U(t)$, which may be obtained in one of two ways. The exact way, as done in Sec. II, is to Fourier transform the frequency-domain phasor to the time domain according to Eq. (8). An approximate approach is to multiply the monochromatic phasor by a temporal Gaussian envelope, as follows:

$$U(\mathbf{r}, t) = U_{BGV}(\mathbf{r}, \omega_0) \exp\left[-i\omega_0 t - \frac{(t - z/c)^2}{\tau^2}\right]. \quad (20)$$

While these two methods may agree for longer pulse durations, it is known that use of a Gaussian temporal envelope as in Eq. (20) fails to correctly model the behavior of ultrashort pulses [36].

The problem may be understood by considering the time-frequency uncertainty relation, i.e., that the spectral bandwidth grows as the pulse length decreases. For sufficiently short pulses, the bandwidth becomes so large that negative frequency components enter with appreciable weight. These nonphysical frequencies may cause the electric fields to grow with transverse distance from the optical axis instead of decay, as required for a physically correct model [41].

A Poisson-like frequency spectrum was used in the derivation of our phasor in Sec. II to correctly model the behavior of ultrashort pulses. Owing to its inherent unit step function $\Theta(\omega)$, a Poisson-like spectrum removes unphysical negative frequency components from the frequency-domain phasor. Thus, upon Fourier transformation into the time domain, one eliminates the possibility of nonphysical temporal fields.

A comparison of the fields calculated from the time-domain phasors defined in Eqs. (8) and (20) for two different pulse durations is given in Fig. 3. As shown in Fig. 3(b) for short pulses, the fields generated from Eq. (20) (subscript "TG") clearly differ from those generated from the Poisson spectrum phasor (subscript "PS"). In contrast, for long pulses, Fig. 3(a) shows much better agreement between the fields generated by the two different methods. This better agreement occurs since the frequency bandwidth of the temporal Gaussian doesn't extend to negative values in the case of a long pulse. Note that the "PS" fields in Fig. 3 are the same as the "pert" fields in Fig. 2.

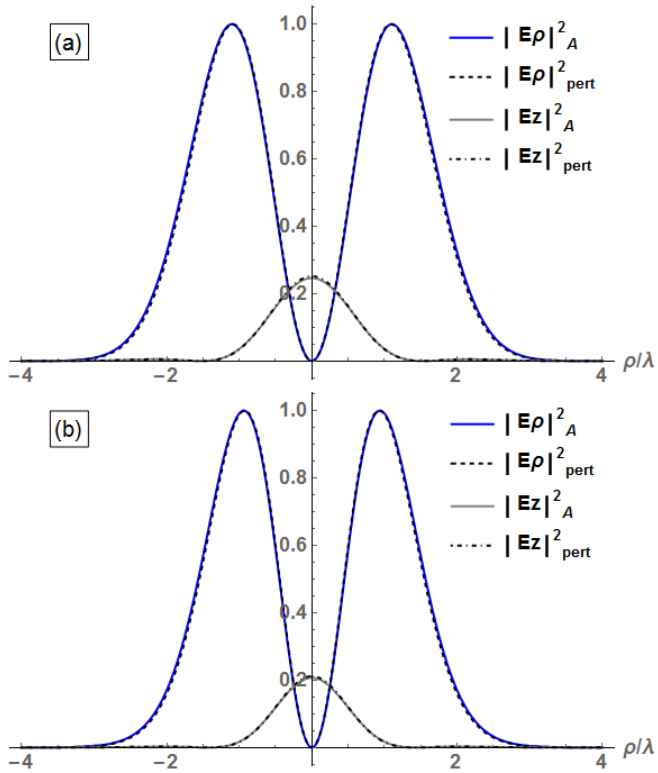

FIG. 2. Comparison of numerical values of the relative intensities of fields E_ρ and E_z near the beam waist for the $LG_{0,0}$ mode for two different spectral parameters: (a) s=2848 ($\sim$20-cycle FWHM, 53.4 fs) or (b) s=7 ($\sim$1-cycle FWHM, 2.65 fs). Solid dark (blue) and light (gray) curves are calculated using fields derived from April's phasor [40] ("A"), while the dashed and dash-dot curves are calculated from the fields given in Eqs. (14) and (16) of this paper with the phasor to perturbative order ϵ_c^2 ("pert"), all with $w_0 = 1.5\lambda$ and $\lambda = 800$ nm ($\epsilon_c^2 \approx 0.0113$).

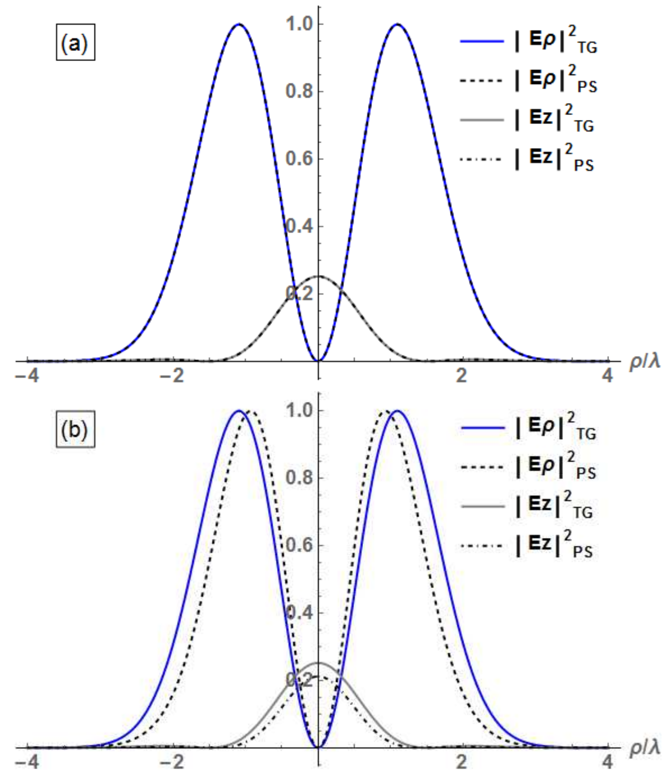

FIG. 3. Comparison of numerical values of the relative intensities of fields E_ρ and E_z near the beam waist for the $LG_{0,0}$ mode for two different spectral parameters: (a) s=2848 ($\sim$20-cycle FWHM, 53.4 fs) or (b) s=7 ($\sim$1-cycle FWHM, 2.65 fs). Solid dark (blue) and light (gray) curves are calculated using the temporal Gaussian ("TG") model of Eq. (20) with the indicated pulse durations, while the dashed and dash-dot curves are calculated using the Fourier transformed Poisson spectrum ("PS") of Eq. (8) to order ϵ_c^2, all with $w_0 = 1.5\lambda$ and $\lambda = 800$ nm ($\epsilon_c^2 \approx 0.0113$).

V. SUMMARY AND CONCLUSIONS

In this paper we have presented an analytic method for calculating the EM fields of a tightly focused, arbitrarily-short laser pulse of any radial and azimuthal LG mode. In brief, the EM fields are obtained from the time-domain phasor, whose analytic expression to the ϵ_c^2 perturbative order is given in Eq. (10). An example for obtaining the phasor to higher orders in ϵ_c^2 is given in Appendix B. For the case of radially-polarized EM fields, Eqs. (13) - (18) show how to obtain the EM fields from the phasor of any perturbative order. With only lowest order perturbative corrections included, these fields are consistent with the field model of April [40] for the Gaussian mode over a wide range of pulse durations. Use of a Poisson-like frequency spectrum was essential to obtain this agreement, as this spectrum eliminates the possibility of negative frequency modes that lead to unphysical fields for ultrashort pulses.

Invoking the condition of isodiffraction is necessary for solving the Fourier integral of the phasor when transforming it into the time domain. The phasor for a completely general nonparaxial eLG beam, valid for arbitrarily short pulses, has never to our knowledge been expressed in the time domain without use of the isodiffraction condition, as otherwise the necessary Fourier integral becomes prohibitively complicated. For nonparaxial complex source-point models, this condition of isodiffraction requires that the imaginary distance to the source point, z_R in this case, remains frequency-independent.

A major benefit of our perturbative model is its scalability to higher radial and orbital LG modes. Expressions for the time-domain EM fields for these higher LG modes using other models usually requires the calculation of infinite sums or the evaluation of integrals involving special functions of complex variables. The integrals over these complex special functions, for arbitrary LG modes, are difficult to evaluate. In our model, all EM fields are written simply in terms of the phasor and its elementary derivatives.

VI. ACKNOWLEDGMENTS

We gratefully acknowledge informative discussions with E. Heyman regarding the nature of isodiffraction. This research is supported in part by the U.S. Department of Energy, Office of Science, Basic Energy Sciences, Division of Chemical Sciences, Geosciences, and Biosciences, under Award No. DE-FG02-96ER14646. It was carried out utilizing the Holland Computing Center of the University of Nebraska, which receives support from the Nebraska Research Initiative.

Appendix A: Derivation of the Factors $f^{(2j)}(v)$

We begin with the frequency-domain phasor, for any LG mode, of BGV in integral form (Eq. (16) of Ref. [22]),

$$U_{n,m} = \int_0^\infty (-\alpha)^{2n+m}(-1)^n \exp(\pm im\phi)\mathrm{w}_0^{2n+m} \times \left[\frac{z_R}{k_z}\exp\left(ik_z(z-iz_R)-kz_R\right)\right] \times J_m(\alpha\rho)\alpha\, d\alpha. \tag{A1}$$

An intermediate result of Ref. [22] is that the phasor of Eq. (A1) above is equivalent to an infinite series representation given by Eq.(22) of Ref. [22],

$$U_{n,m} = \int_0^\infty (-\alpha)^{2n+m}(-1)^n \exp(\pm im\phi)\mathrm{w}_0^{2n+m} \times \left[\frac{\mathrm{w}_0^2}{2}\exp(ikz)\exp\left(-\frac{i\alpha^2}{2k}(z-iz_R)\right) \sum_{j=0}^{\infty}\frac{G^{(2j)}}{(k\mathrm{w}_0)^{(2j)}}\right] J_m(\alpha\rho)\alpha\, d\alpha. \tag{A2}$$

Comparing these two equations, it is clear that the terms inside the square brackets of each expression must be equal. Making use of the relation $z_R = k\mathrm{w}_0^2/2$ and our previous definition of β from Eq. (1), and defining $\Omega \equiv \mathrm{w}_0^2 k_\perp^2$, the terms in square brackets of Eqs. (A1) and (A2) can be equated and solved for the infinite sum, yielding

$$\sum_{j=0}^{\infty}\epsilon^{(2j)}G^{(2j)} = \frac{1}{\sqrt{1-\epsilon^2\Omega}}\exp\left(\frac{\sqrt{1-\epsilon^2\Omega}-1}{2\epsilon^2\beta}+\frac{\Omega}{4\beta}\right) \tag{A3}$$

In the above expression, we again define $\epsilon \equiv 1/(k\mathrm{w}_0)$ since the description at this point is monochromatic. The RHS can then be expanded in a Taylor series about $\epsilon^2 = 0$. Collecting powers of ϵ^2 in this expansion yields the perturbative terms $G^{(2j)}$,

$$\sum_{j=0}^{\infty}\epsilon^{(2j)}G^{(2j)} = O\left(\epsilon^8\right) + 1 + \epsilon^2\left(\frac{\Omega}{2}-\frac{\Omega^2}{16\beta}\right) + \epsilon^4\left(\frac{3\Omega^2}{8}-\frac{\Omega^3}{16\beta}+\frac{\Omega^4}{512\beta^2}\right) + \epsilon^6\left(\frac{5\Omega^3}{16}-\frac{15\Omega^4}{256\beta}+\frac{3\Omega^5}{1024\beta^2}-\frac{\Omega^6}{24576\beta^3}\right). \tag{A4}$$

These results confirm Eq. (23) of Ref. [22], and elucidate how to extend the method to arbitrarily large j. These terms $G^{(2j)}$ are then used in Eq. (A2) along with the integral

$$\int_0^\infty \alpha^{2n+m}\exp\left(-p^2\alpha^2\right)J_m(\alpha\rho)\alpha\, \mathrm{d}\alpha = \frac{n!}{2}p^{-(2n+m+2)}\left(\frac{\rho}{2p}\right)^m L_n^m\left(\frac{\rho^2}{4p^2}\right)\exp\left(-\frac{\rho^2}{4p^2}\right) \tag{A5}$$

to produce the factors $f^{(2j)}(v)$ given by BGV in Ref. [22].

Appendix B: The Phasor to order ϵ_c^4

In this Appendix we derive the $O(\epsilon_c^4)$ correction to the time-domain phasor, starting with the frequency-domain phasor in Eq. (1). Considering only the term of order ϵ^4 in Eq. (1), we make the replacements $\mathrm{w}_0 \to \sqrt{2z_R/k}$ and $k \to \omega/c$ and invoke the condition of isodiffraction, which requires that z_R is constant. We obtain

$$\frac{\epsilon_c^4}{\beta^2}U_{4,BGV} = (-1)^{n+m}2^{2n+m}\exp(i\omega z/c + im\phi) \times h^{2n+m+2}v^{m/2}\exp(-v)\left[\left(\frac{c}{2\omega\beta z_R}\right)^2 \times \left\{6(n+2)!L_{n+2}^m(v) - 4(n+3)!L_{n+3}^m(v) + \frac{1}{2}(n+4)!L_{n+4}^m(v)\right\}\right]. \tag{B1}$$

Multiplying this result by the Poisson-like frequency spectrum in Eq. (5), expressing the associated Laguerre polynomials as sums [see Eqs. (3) and (4)], and extracting powers of ω within the sums, we obtain

$$U_4(\omega) = \frac{\Lambda_{n,m}}{\Gamma(s+1)}\exp\left\{-\omega\left(-\frac{iz}{c}+\xi+\frac{s}{\omega_0}\right)\right\} \times \left(\frac{s}{\omega_0}\right)^{s+1}\frac{\theta(\omega)\sqrt{2\pi}\epsilon_c^4}{\beta^2}\left[\sum_{j=0}^{n+2}\widetilde{c_{2,2}}\,\xi^j\omega^{\gamma-2} - \sum_{j=0}^{n+3}\widetilde{c_{2,3}}\,\xi^j\omega^{\gamma-2} + \sum_{j=0}^{n+4}\widetilde{c_{2,4}}\,\xi^j\omega^{\gamma-2}\right], \tag{B2}$$

where some variables defined in Eq. (11) have been used, and new constants are defined as follows:

$$\widetilde{c_{2,2}} \equiv 6\omega_0^2(n+2)(n+1)G_{(n+2),m,j} \tag{B3a}$$
$$\widetilde{c_{2,3}} \equiv 4\omega_0^2(n+3)(n+2)(n+1)G_{(n+3),m,j} \tag{B3b}$$
$$\widetilde{c_{2,4}} \equiv \frac{\omega_0^2}{2}(n+4)(n+3)(n+2)(n+1) \tag{B3c}$$
$$\times\, G_{(n+4),m,j}. \tag{B3d}$$

We now Fourier transform $U_4(\omega)$ to the time domain as in Eq. (8) to obtain $U_4(t)$,

$$\begin{aligned} U_4(t) = \frac{\Lambda_{n,m}}{\Gamma(s+1)}\left(\frac{s}{\omega_0}\right)^{s+1}\frac{\epsilon_c^4}{\beta^2}\int_0^\infty \exp(-\omega\eta) \\ \left[\sum_{j=0}^{n+2}\widetilde{c_{2,2}}\;\xi^j\omega^{\gamma-2} - \sum_{j=0}^{n+3}\widetilde{c_{2,3}}\;\xi^j\omega^{\gamma-2}\right. \\ \left. + \sum_{j=0}^{n+4}\widetilde{c_{2,4}}\;\xi^j\omega^{\gamma-2}\right]\mathrm{d}\omega\,, \end{aligned} \tag{B4}$$

where $\eta = -iz/c + \xi + s/\omega_0 + it$. Using the integral representation of the gamma function in Eq. (9), we obtain

$$\begin{aligned} U_4 \;&= \Lambda_{n,m}\left(\frac{s}{\omega_0}\right)^{s+1}\frac{\epsilon_c^4}{\beta^2}\left[\sum_{j=0}^{n+2}\overline{c_{2,2}}\;\xi^j\eta^{-(\gamma-1)}\right. \\ &\left. -\sum_{j=0}^{n+3}\overline{c_{2,3}}\;\xi^j\eta^{-(\gamma-1)} + \sum_{j=0}^{n+4}\overline{c_{2,4}}\;\xi^j\eta^{-(\gamma-1)}\right], \end{aligned} \tag{B5}$$

where $\overline{c_{2,\delta}} \equiv \widetilde{c_{2,\delta}}\Gamma(\gamma-1)/\Gamma(s+1)$ for $\delta = 2, 3, 4$.

Taking now the overall prefactor $(s/\omega_0)^{s+1}$ in Eq. (B5) inside each of the sums and using the definition of T in Eq. (11)(b), we can write for any power q,

$$\left(\frac{s}{\omega_0}\right)^{s+1}\eta^{-q} = \left(\frac{s}{\omega_0}\right)^{s+1-q}T^{-q}. \tag{B6}$$

Defining the coefficients $c_{2,\delta} \equiv \overline{c_{2,\delta}}(s/\omega_0)^{(s+2-\gamma)}$ for $\delta = 2, 3, 4$, the final result for the $O(\epsilon_c^4)$ term $U_4(t)$ is:

$$\begin{aligned} U_4 \;&= \Lambda_{n,m}\frac{\epsilon_c^4}{\beta^2}\left[\sum_{j=0}^{n+2}c_{2,2}\;\xi^jT^{-(\gamma-1)}\right. \\ &\left. -\sum_{j=0}^{n+3}c_{2,3}\;\xi^jT^{-(\gamma-1)} + \sum_{j=0}^{n+4}c_{2,4}\;\xi^jT^{-(\gamma-1)}\right]. \end{aligned} \tag{B7}$$

Adding this result to the $O(\epsilon_c^2)$ phasor $U^{(2)}$ in Eq. (10), the complete $O(\epsilon_c^4)$ time-domain phasor $U^{(4)}(t)$ is:

$$\begin{aligned} U^{(4)} = \Lambda_{n,m}\Bigg[&\sum_{j=0}^{n}c_{0,0}\xi^jT^{-(\gamma+1)} \\ &+\frac{\epsilon_c^2}{\beta}\left(\sum_{j=0}^{n+1}c_{1,1}\xi^jT^{-\gamma} - \sum_{j=0}^{n+2}c_{1,2}\xi^jT^{-\gamma}\right) \\ &+\frac{\epsilon_c^4}{\beta^2}\left(\sum_{j=0}^{n+2}c_{2,2}\;\xi^jT^{1-\gamma} - \sum_{j=0}^{n+3}c_{2,3}\;\xi^jT^{1-\gamma}\right. \\ &\left.+\sum_{j=0}^{n+4}c_{2,4}\;\xi^jT^{1-\gamma}\right)\Bigg]. \end{aligned} \tag{B8}$$

The calculation of higher order terms would proceed similarly. The upper limits of the sums, their interior coefficients, the leading powers of ϵ_c^2/β, and the integrated powers of ω would change, but otherwise the process would be identical to that demonstrated above.

Appendix C: Radius of Convergence of the Perturbative Phasor

Perturbative models require that higher-order terms in the perturbative expansion have smaller magnitude than lower-order terms, so that the infinite series converges. However, the series expansions upon which such perturbations are based often do not have this behavior in all space. For example, the one-dimensional function $1/(x^2+1)$ is well-defined at all values on the real axis. Expanding this function in a Maclaurin series gives $1 - x^2 + x^4 + ...$ which only converges in the finite region $|x| < 1$, rendering the series expansion useless outside this radius of convergence. In this appendix, we estimate the radius of convergence for the perturbative phasor in Eq. (1) of this paper.

We begin by considering the magnitude of the frequency-domain phasor in Eq. (1). Each term in the perturbative sum contains a factor $f_{n,m}^{(2j)}(v)$, derived in Appendix A, which is a sum of associated Laguerre polynomials. At some perturbative order j, the dominant contribution to $f_{n,m}^{(2j)}(v)$ is

$$f_{n,m}^{(2j)}(v) \approx \frac{(n+2j)!}{j!}L_{n+2j}^m(v), \tag{C1}$$

since $L_{n+2j}^m(v)$ has the highest power of v amongst all associated Laguerre polynomials contributing to $f_{n,m}^{(2j)}(v)$ [cf. Eqs. (2) and (3)]. The term in $L_{n+2j}^m(v)$ having the highest power of v is $G_{(n+2j,m,n+2j)}v^{n+2j}$ [cf. Eq. (3)]. Making use of Eq. (4), and noting that $|h| = (1+z^2/z_R^2)^{-1/4}$, one can write the magnitude of the dominant contribution to the j^{th}-order term of Eq. (1) as

$$|U^{(2j)}| \approx \frac{2^{2n+m}\epsilon^{2j}}{j!}\left(1+\frac{z^2}{z_R^2}\right)^{-\frac{1}{2}(2n+3j+m+1)} \times \exp\left[-\frac{\rho^2}{\mathrm{w}_0^2\,(1+z^2/z_R^2)}\right]\left(\frac{\rho}{\mathrm{w}_0}\right)^{2n+4j+m}. \tag{C2}$$

As noted above, the radius of convergence is defined by the spatial region in which the term of order j is smaller than the term of order $j-1$. To find such a region, we calculate the difference $|U^{(2j)}| - |U^{(2j-2)}| < 0$. Given that $\rho \geq 0$ and $z^2 \geq 0$, this inequality can only be satisfied for

$$\rho < \left[j\left(1+\frac{z^2}{z_R^2}\right)^{3/2}\frac{\mathrm{w}_0^4}{\epsilon^2}\right]^{1/4}. \tag{C3}$$

This condition must be satisfied for all j, and the maximum allowed value of ρ increases with larger j. Therefore, the radius of convergence ρ_c is determined by the minimal case of $j=1$,

$$\rho < \left[\left(1+\frac{z^2}{z_R^2}\right)^{3/2}\frac{\mathrm{w}_0^4}{\epsilon^2}\right]^{1/4} \equiv \rho_c. \tag{C4}$$

Note that ρ_c is defined for any z and is independent of the LG modes n and m.

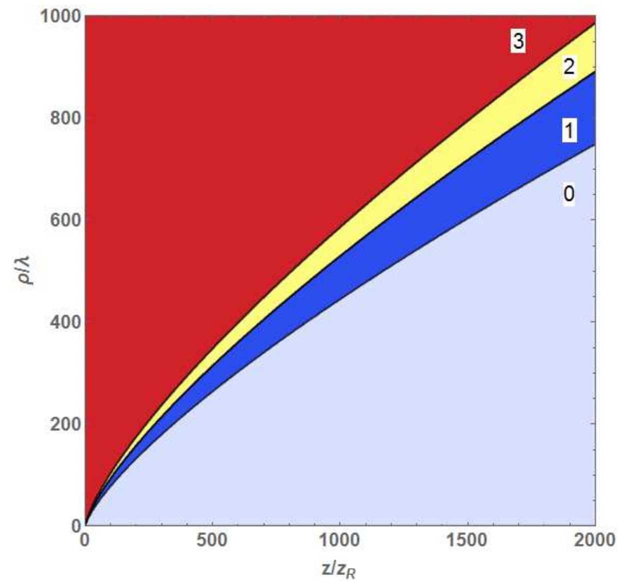

FIG. 4. Illustration of the radius of convergence for the phasor in Eq. (1), demonstrated by the dominant perturbative order j as a function of spatial location. Each region is labelled by the perturbative order $j \in [0,3]$ that is largest therein. The region in which the $j=0$ term dominates is the region in which the perturbation is converged. This plot was made using $\mathrm{w}_0 = \lambda = 800$ nm [$\epsilon = 1/(2\pi)$].

This radius of convergence is demonstrated in Fig. 4, wherein the magnitude of the perturbative phasor given in Eq. (C2) is plotted as a function of ρ and z for up to three orders of perturbative correction. The minimum radius of convergence ρ_c is given in Eq. (C4), which corresponds to the line between regions 0 and 1 in Fig. 4. The space with ρ-values below this line corresponds to the region of perturbative convergence, or the region in which the 0^{th}-order phasor is dominant.

[1] G. Molina-Terriza, J. P. Torres, and L. Torner, "Twisted photons," Nat. Phys. **3**, 305 (2007).

[2] A. M. Yao and M. J. Padgett, "Orbital angular momentum: origins, behavior and applications," Adv. Opt. Photonics **3**, 161 (2011).

[3] L. Allen and M. Padgett, "The Orbital Angular Momentum of Light: An Introduction," in *Twisted Photons: Applications of Light with Orbital angular Momentum*, edited by J. P. Torres and L. Torner (Wiley-VCH Verlag GmbH & Co., Weinheim, Germany, 2011), pp. 1–12.

[4] C. Hernández-García, J. Vieira, J. Mendonça, L. Rego, J. San Román, L. Plaja, P.R. Ribic, D. Gauthier, and A. Picón, "Generation and Applications of Extreme-Ultraviolet Vortices," Photonics **4**, 28 (2017).

[5] S. M. Lloyd, *Electron Beams with Orbital Angular Momentum*, Ph.D. thesis, University of York, U.K. (2013).

[6] K. Y. Bliokh, I. P. Ivanov, G. Guzzinati, L. Clark, R. Van Boxem, A. Béché, R. Juchtmans, M. A. Alonso, P. Schattschneider, F. Nori, and J. Verbeeck, "Theory and applications of free-electron vortex states," Phys. Rep. **690**, 1 (2017), 1703.06879.

[7] S. M. Lloyd, M. Babiker, G. Thirunavukkarasu, and J. Yuan, "Electron vortices: Beams with orbital angular momentum," Rev. Mod. Phys. **89**, 035004 (2017).

[8] K. A. Forbes and D. L. Andrews, "Optical orbital angular momentum: twisted light and chirality," Opt. Lett. **43**, 435 (2018).

[9] A. Afanasev, C. E. Carlson, C. T. Schmiegelow, J. Schulz, F. Schmidt-Kaler, and M. Solyanik, "Experimental verification of position-dependent angular-momentum selection rules for absorption of twisted light by a bound electron," New J. Phys. **20**, 023032 (2018).

[10] M. Vaziri, M. Golshani, S. Sohaily, and A. Bahrampour, "Electron acceleration by linearly polarized twisted laser pulse with narrow divergence," Phys. Plasmas **22**, 033118 (2015).

[11] Q. Xiao, C. Klitis, S. Li, Y. Chen, X. Cai, M. Sorel, and S. Yu, "Generation of photonic orbital angular momentum superposition states using vortex beam emitters with superimposed gratings," Opt. Express **24**, 3168 (2016).

[12] C. Hernández-García, A. Picón, J. San Román, and L. Plaja, "Attosecond Extreme Ultraviolet Vortices from

High-Order Harmonic Generation," Phys. Rev. Lett. **111**, 083602 (2013).

[13] L. Rego, J. San Román, A. Picón, L. Plaja, and C. Hernández-García, "Nonperturbative Twist in the Generation of Extreme-Ultraviolet Vortex Beams," Phys. Rev. Lett. **117**, 163202 (2016).

[14] A. Turpin, L. Rego, A. Picón, J. San Román, and C. Hernández-García, "Extreme Ultraviolet Fractional Orbital Angular Momentum Beams from High Harmonic Generation," Sci. Rep. **7**, 43888 (2017).

[15] B. Richards and E. Wolf, "Electromagnetic Diffraction in Optical Systems. II. Structure of the Image Field in an Aplanatic System," Proc. R. Soc. A **253**, 358 (1959).

[16] M. Lax, W. H. Louisell, and W. B. McKnight, "From Maxwell to paraxial wave optics," Phys. Rev. A **11**, 1365 (1975).

[17] L. W. Davis, "Theory of electromagnetic beams," Phys. Rev. A **19**, 1177 (1979).

[18] G. P. Agrawal and D. N. Pattanayak, "Gaussian beam propagation beyond the paraxial approximation," J. Opt. Soc. Am. **69**, 575 (1979).

[19] J. P. Barton and D. R. Alexander, "Fifth-order corrected electromagnetic field components for a fundamental Gaussian beam," J. Appl. Phys. **66**, 2800 (1989).

[20] Y. I. Salamin, "Fields of a Gaussian beam beyond the paraxial approximation," Appl. Phys. B **86**, 319 (2007).

[21] S. R. Seshadri, "Virtual source for a Laguerre-Gauss beam." Opt. Lett. **27**, 1872 (2002).

[22] M. A. Bandres and J. C. Gutiérrez-Vega, "Higher-order complex source for elegant Laguerre-Gaussian waves." Opt. Lett. **29**, 2213 (2004).

[23] M. Couture and P. A. Belanger, "From Gaussian beam to complex-source-point spherical wave," Phys. Rev. A **24**, 355 (1981).

[24] T. Takenaka, M. Yokota, and O. Fukumitsu, "Propagation of light beams beyond the paraxial approximation," J. Opt. Soc. Am. A **2**, 826 (1985).

[25] E. Zauderer, "Complex argument Hermite-Gaussian and Laguerre-Gaussian beams," J. Opt. Soc. Am. A **3**, 465 (1986).

[26] P. Favier, K. Dupraz, K. Cassou, X. Liu, A. Martens, C. F. Ndiaye, T. Williams, and F. Zomer, "Short pulse laser beam beyond paraxial approximation," J. Opt. Soc. Am. A **34**, 1351 (2017).

[27] S. Y. Shin and L. B. Felsen, "Gaussian beam modes by multipoles with complex source points," J. Opt. Soc. Am. **67**, 699 (1977).

[28] Z. Ulanowski and I. K. Ludlow, "Scalar field of nonparaxial Gaussian beams," Opt. Lett. **25**, 1792 (2000).

[29] M. V. Berry, "Evanescent and real waves in quantum billiards and Gaussian beams," J. Phys. A. Math. Gen. **27**, L391 (1994).

[30] C. J. R. Sheppard and S. Saghafi, "Beam modes beyond the paraxial approximation: A scalar treatment," Phys. Rev. A **57**, 2971 (1998).

[31] A. April, "Nonparaxial elegant Laguerre-Gaussian beams," Opt. Lett. **33**, 1392 (2008).

[32] J. Lekner, "TM, TE and 'TEM' beam modes: exact solutions and their problems," J. Opt. A: Pure Appl. Opt. **3**, 407 (2001).

[33] C. J. R. Sheppard, "Comment on 'TM, TE and 'TEM' beam modes: exact solutions and their problems'," J. Opt. A: Pure Appl. Opt. **4**, 217 (2002).

[34] J. Lekner, "Reply to 'Comment on "TM, TE and 'TEM' beam modes: exact solutions and their problems"'," J. Opt. A: Pure Appl. Opt. **4**, 219 (2002).

[35] S. Saghafi and C. J. R. Sheppard, "Near field and far field of elegant Hermite-Gaussian and Laguerre-Gaussian modes," J. Mod. Opt. **45**, 1999 (1998).

[36] M. A. Porras, "Ultrashort pulsed Gaussian light beams," Phys. Rev. E **58**, 1086 (1998).

[37] J.-Y. Lu and J. Greenleaf, "Nondiffracting X Waves–Exact Solutions to Free-Space Scalar Wave Equation and Their Finite Aperture Realizations," IEEE Trans. Ultrason. Ferroelectr. Freq. Control **39**, 19 (1992).

[38] C. J. R. Sheppard, "Bessel pulse beams and focus wave modes," J. Opt. Soc. Am. A **18**, 2594 (2001).

[39] K. J. Parker and M. A. Alonso, "Longitudinal iso-phase condition and needle pulses," Opt. Express **24**, 28669 (2016).

[40] A. April, "Ultrashort, Strongly Focused Laser Pulses in Free Space," in *Coherence and Ultrashort Pulse Laser Emission*, edited by F. J. Duarte (InTech, 2010) Chap. 16, pp. 355–382.

[41] C. F. R. Caron and R. M. Potvliege, "Free-space propagation of ultrashort pulses: Space-time couplings in Gaussian pulse beams," J. Mod. Opt. **46**, 1881 (1999).

[42] S. Feng and H. G. Winful, "Spatiotemporal structure of isodiffracting ultrashort electromagnetic pulses," Phys. Rev. E **61**, 862 (2000).

[43] J. D. Jackson, *Classical Electrodynamics* (Wiley, 1995), p. 280.

[44] J. A. Stratton, *Electromagnetic Theory* (McGraw-Hill, 1941), p. 28.

[45] A. Vikartofsky, L.-W. Pi, and A. F. Starace, "Discontinuities in the electromagnetic fields of vortex beams in the complex source-sink model," Phys. Rev. A **95**, 053826 (2017).

[46] A. E. Siegman, *Lasers* (University Science Books, Mill Valley, CA, 1986), p. 102.

[47] S. Hassani, *Mathematical Methods: For Students of Physics and Related Fields, 2nd. Ed.* (Springer, New York, 2009).

[48] Z. Wang, Z. Zhang, Z. Xu, and Q. Lin, "Space-time profiles of an ultrashort pulsed Gaussian beam," IEEE J. Quantum Electron. **33**, 566 (1997).

[49] M. Abramowitz and I. A. Stegun, *Handbook of Mathematical Functions* (Dover Publications, New York, 1972).